

Energy Level Engineering in Organic Thin Films by Tailored Halogenation

Katrin Ortstein,* Sebastian Hutsch, Alexander Hinderhofer, Jörn Vahland, Martin Schwarze, Sebastian Schellhammer, Martin Hodas, Thomas Geiger, Hans Kleemann, Holger F. Bettinger, Frank Schreiber, Frank Ortman, and Karl Leo

In modern electronics, it is essential to adapt band structures by adjusting energy levels and band gaps. At first sight, this “band structure engineering” seems impossible in organic semiconductors, which usually exhibit localized electronic states instead of Bloch bands. However, the strong Coulomb interaction in organic semiconductors allows for a continuous shift of the ionization energy (IE) over a wide range by mixing molecules with halogenated derivatives that exhibit different quadrupole moments. Here, this effect of energy level engineering on blends of pentacene and two fluorinated derivatives, in which the position but not the number of fluorine atoms differ, is studied. Structural investigations confirm that pentacene forms intermixed phases in blends with the fluorinated species. The investigation of electronic properties and simulations reveals a much larger shift of the ionization energy (1.5 eV) than in previous studies, allowing to test this model in a range not investigated so far, and emphasizing the role of the position of the halogen atoms. The tuning effect is preserved in electronic devices such as field-effect transistors and significantly influences device characteristics.

1. Introduction

Organic semiconductors are rapidly entering everyday life, for example, as organic light emitting diode displays in smartphones and TVs, as solar cells on our rooftops, or as organic transistors in flexible displays or smart tags. In order to produce efficient components, it is indispensable in modern electronics to adapt the electronic energy levels and the energy gap of the semiconductor materials and thus to be able to produce almost any desired band structures. In inorganic semiconductors, this is accomplished by blending compound semiconductors such as GaAs with AlAs (see, e.g., Sze).^[1] However, for this approach, delocalized electronic states, that is, Bloch-waves are required to “average” over the different constituents. Since organic semiconductors usually have localized

electronic states instead of energy bands, this band structure engineering based on Bloch-waves does not seem to be possible for organic electronics. Instead, organic molecules offer the possibility to vary the electronic properties of the semiconductor by changing the structure of the molecules. However, even small changes in electronic properties require elaborate synthesis of new molecules, often resulting in unwanted changes in other molecular and thin-film properties. In this regard, it is quite surprising that the ionization energy (IE) and the electron affinity (EA) of organic semiconductors can still be tuned over a wide energy range by simply mixing them with halogenated derivatives.^[2,3] This tuning mechanism is based on interactions of excess charge carriers with the quadrupole electrostatic field of the molecules surrounding them and opens interesting new perspectives for applications, such as the fine-tuning of open circuit voltages in organic solar cells.

In literature, blended layers of sterically similar molecules have been investigated extensively. Many of these publications focus on donor–acceptor systems, for example, with phthalocyanines or acenes with halogenated derivatives, and their use in organic solar cells. They mostly address the structural^[4–10] and the optical properties^[4–6,8,11] of the blends, but also the energy landscape^[12] and electrical properties such as the charge carrier mobility^[4,5] have been considered.

K. Ortstein, J. Vahland, Dr. M. Schwarze, Dr. H. Kleemann, Prof. K. Leo
Dresden Integrated Center for Applied Physics and Photonic Materials
(IAPP) and Institute for Applied Physics
Technische Universität Dresden
Dresden 01062, Germany
E-mail: katrin.ortstein@tu-dresden.de

S. Hutsch, S. Schellhammer, Dr. F. Ortman
Center for Advancing Electronics Dresden
Technische Universität Dresden
Dresden 01062, Germany

Dr. A. Hinderhofer, Dr. M. Hodas, Prof. F. Schreiber
Institut für Angewandte Physik
Eberhard-Karls-Universität Tübingen
Auf der Morgenstelle 10, Tübingen 72076, Germany

T. Geiger, Prof. H. F. Bettinger
Institut für Organische Chemie
Eberhard-Karls-Universität Tübingen
Auf der Morgenstelle 18, Tübingen 72076, Germany

 The ORCID identification number(s) for the author(s) of this article can be found under <https://doi.org/10.1002/adfm.202002987>.

© 2020 The Authors. Published by WILEY-VCH Verlag GmbH & Co. KGaA, Weinheim. This is an open access article under the terms of the Creative Commons Attribution License, which permits use, distribution and reproduction in any medium, provided the original work is properly cited.

DOI: 10.1002/adfm.202002987

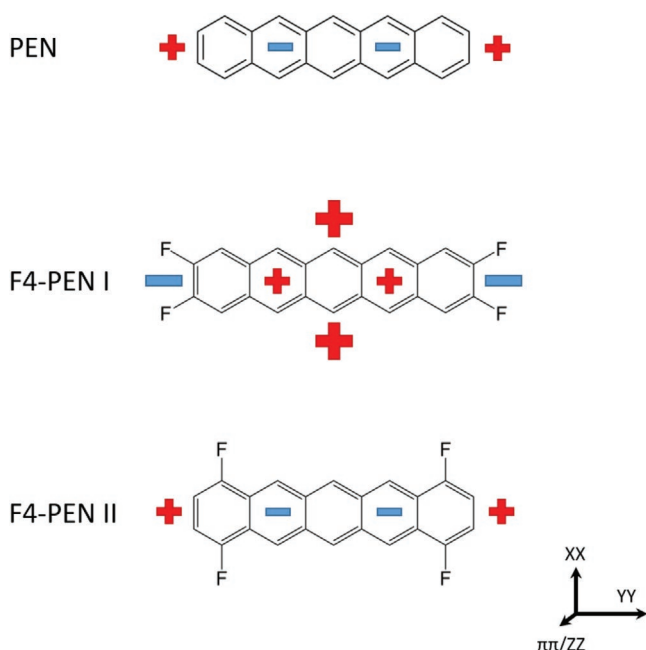


Figure 1. Molecular structures of PEN, F4-PEN I, and F4-PEN II and schematic distribution of the main quadrupole moments Q . Small (large) symbols correspond to $Q \geq 20 \text{ ea}_0^2$ ($Q \geq 50 \text{ ea}_0^2$). The Q_z components are indicated by the symbols in the center of the molecules.

In this work, we extend the concept of energy level engineering to blends that differ only in the position of halogen atoms of one molecule but have the same molecular formula, that is, only few atoms change their position. In particular, we use various experimental and theoretical methods to study two new fourfold fluorinated pentacene derivatives (F4-PEN I and F4-PEN II) in combination with the widely used pentacene (PEN) (Figure 1), allowing to study the influence of the position of the halogenation in a molecule instead of the degree of halogenation. F4-PEN I and F4-PEN II exhibit almost identical calculated gas phase ionization energies IE_0 . Still the IE in blends of a fluorinated compound with pentacene differs substantially for both compounds with energy differences exceeding 1 eV in ultraviolet photoelectron spectroscopy (UPS). The combination PEN:F4-PEN I yields a new record in the shift in IE, showing that the quadrupole effect can be scaled to a much larger energy range than presented before. Moreover, we show that this shift of the energy levels is relevant for electronic devices such as organic field-effect transistors, where the injection of charge carriers is mainly governed by the difference between the work function of the metallic electrodes and the IE of the semiconductor material.

Table 1. Overview over the quadrupole moment components Q_i , the calculated gas phase ionization energy IE_0 , and the measured thin-film ionization energy IE for the used PEN derivatives.

Material	$Q_x [\text{ea}_0^2]$	$Q_y [\text{ea}_0^2]$	$Q_z [\text{ea}_0^2]$	$IE_0 [\text{eV}]$	IE (max) [eV]
PEN	18.03	23.82	-41.85	6.51	5.51
F4-PEN I	64.49	-76.08	11.60	6.91	7.15
F4-PEN II	-13.81	33.92	-20.15	6.95	5.87

The values for IE_0 are calculated with density functional theory (see Experimental Section). For IE we use the maximum position of the HOMO region instead of the onset.

PEN and F4-PEN I are high-mobility transport material and devices based on blended layers confirm the findings of the energy level shift qualitatively. Our study emphasizes the importance of electron withdrawing substituents and their respective positions for the energy levels in electronic devices.

2. Results and Discussion

2.1. Simulation of Molecular Properties

The new fluorinated pentacene derivatives studied here differ only in the position of the fluorine atoms (Figure 1). While in the first derivative (2,3,9,10-tetrafluoropentacene, F4-PEN I),^[13–16] the fluorine atoms substitute the terminating hydrogens at the molecular long-axis, in the second derivative (1,4,8,11-tetrafluoropentacene, F4-PEN II),^[17] the substitution sites are shifted by one atom each toward the center. In addition to their similar molecular structure, the three molecules also exhibit similar gas phase ionization energies IE_0 , which we simulate with density functional theory (see Experimental Section). The presence of the four fluorine atoms increases IE_0 by 0.40 eV for F4-PEN I and 0.44 eV for F4-PEN II (Table 1). Despite the small difference in the IE_0 between the two derivatives, the fluorine atoms and their positions have an immense impact on the charge distribution on the molecules, because of their electron attracting nature, which is schematically shown in Figure 1. To quantify this difference, we calculate the molecular quadrupole moments (cf. Table 1). PEN and F4-PEN II show comparable values for the three directions, while all the quadrupole moments of F4-PEN I differ considerably from the ones of PEN, being more positive in x and z direction and more negative in y direction. We thus expect that the crystal field generated by F4-PEN I molecules significantly differs from the crystal field generated by PEN and F4-PEN II molecules.

Since changes in the molecular quadrupole moment can affect the ionization energies in the solid state (IE), we expect to shift the ionization energies of the individual compounds in the blend layers by mixing F4-PEN I with PEN (and analogously F4-PEN II with PEN). The range of the potential shift depends on the material combination and the corresponding difference between the quadrupole moments of the molecules. Therefore, the combination of F4-PEN I with PEN seems to be most promising for this effect of energy level tuning. However, in order to realize this shift of the energy levels, the different types of molecules should interact on a length scale of a few nm. Therefore, a good

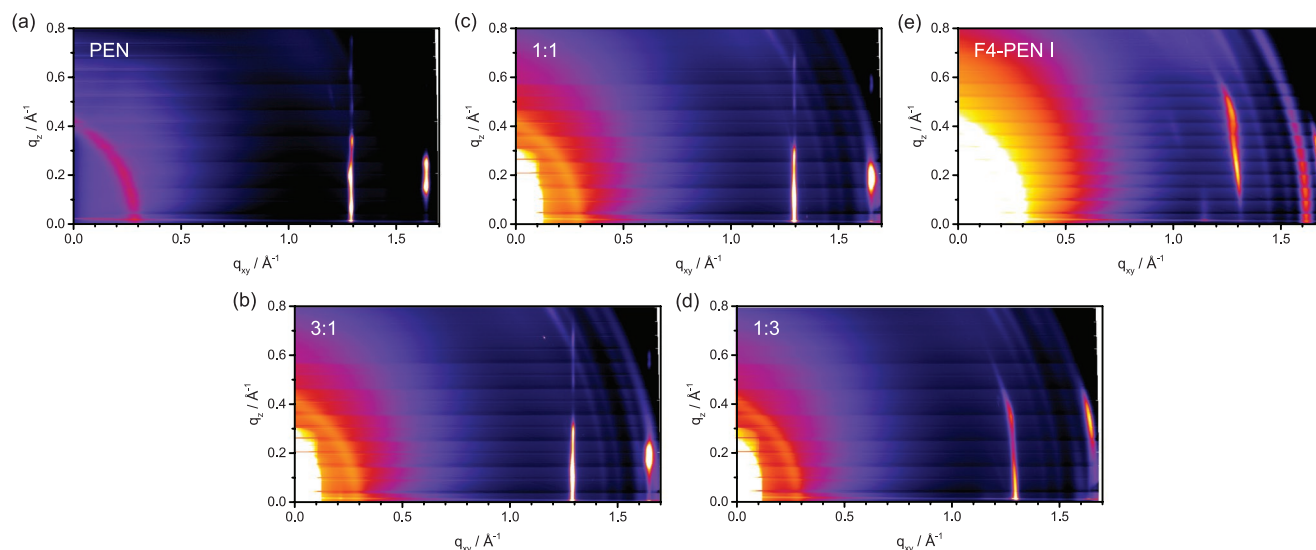


Figure 2. GIWAXS data of PEN, F4-PEN I, and three mixtures. There are no pure PEN and F4-PEN I phases visible in the mixtures and the unit cells change continuously, implying that both compounds are intermixing without phase separation.

intermixing down to the scale of neighboring molecules is preferred.^[3,18]

2.2. Structural Investigations

We perform structural characterization of the blends with grazing incidence wide-angle X-ray scattering (GIWAXS) measurements, focusing on the more promising PEN:F4-PEN I blends. We measure GIWAXS on five samples with different material compositions. Two samples consisting of the pure materials PEN and F4-PEN I, and three blends are studied with molar mixing ratios of 3:1, 1:1, and 1:3, respectively (Figure 2, Table 2), grown on silicon oxide substrates. The lattice parameters of PEN correspond to those published,^[19] that is, it has a crystalline structure with its ab-plane parallel to the substrate. Pure F4-PEN I is also crystalline (Figure 2e). The ab-plane is likely tilted relative to the substrate, which results in weak ordering in the out-of-plane direction (no peak in standard 2θ geometry). The mixed films have slightly different unit cells compared to PEN with increased volume for higher F4-PEN I content (see lattice parameters in Table 2). The ab-plane is always oriented parallel to the substrate. With increasing F4-PEN I content, the mosaicity is increasing, that is, more and more unit cells are slightly tilted with respect to the substrate. This is visible

from the “ring-like” smearing of unit cells for increased F4-PEN I content. Since we cannot detect the pure PEN and F4-PEN I phases in the mixtures and the unit cells are continuously changing, we conclude that both compounds are mixing without phase separation. The increase of unit cell volume with higher F4-PEN I content is consistent with this observation. Thus, the structural properties of the blends are promising for energy level engineering.

2.3. Measurements of the Ionization Energy of Blended Films

Next, we investigate the behavior of the ionization energy in the blends. Figure 3 shows the peak positions of the highest occupied molecular orbital (HOMO) distribution determined with UPS for PEN (red squares), F4-PEN I (blue dots, Figure 3a), and F4-PEN II (blue dots, Figure 3b) as a function of the PEN content in the blend. Both combinations exhibit a linear shift of the IE for both of the materials in the blends, however with strongly different slopes. While for PEN:F4-PEN I, the individual IEs are shifted by more than 1 eV, the shift is very weak for PEN:F4-PEN II with 0.1 eV. Consequently, for the combination of PEN and F4-PEN I, the IEs of the pure materials differ by 1.64 eV while the IEs of PEN and F4-PEN II differ only by 0.36 eV (cf. Table 1). In addition, the difference between the IEs of the fluorinated and unfluorinated compounds changes

Table 2. Unit cells of PEN:F4-PEN I mixtures. The estimated error bars are ± 0.03 Å for the unit cell lengths and $\pm 0.2^\circ$ for the unit cell angles due to only few visible reflections.

	a [Å]	b [Å]	c [Å]	α [°]	β [°]	γ [°]	Vol. [Å ³]	Comment
PEN	5.96	7.6	15.6	81.3	86.6	89.8	697	ab—parallel to substrate
3:1	5.98	7.63	16.4	82.3	89.5	90	742	ab—parallel to substrate
1:1	6	7.61	16.7	82.8	89.2	90	756	ab—parallel to substrate
1:3	6	7.6	17.5	90	90	90	798	ab—parallel to substrate
F4-PEN I								

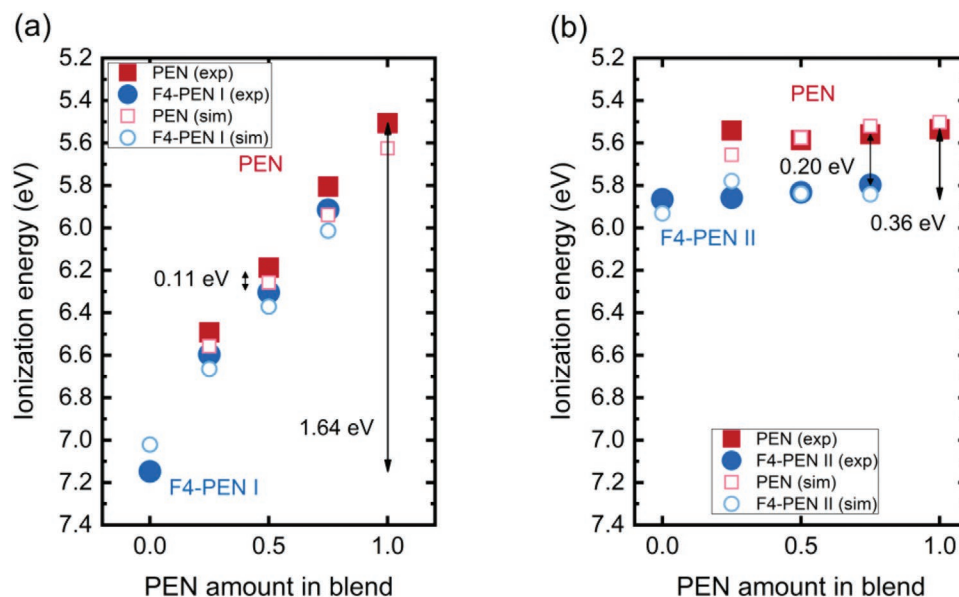


Figure 3. Experimental and simulated behavior of the IEs of a) PEN and F4-PEN I as well as b) PEN and F4-PEN II as function of the amount of PEN in the blends. The measured values represent the maximum positions of the HOMO distributions plotted in Figure S1, Supporting Information.

with the environment. In the PEN:F4-PEN II blends, this difference is rather small with only 0.20 eV and is further reduced to 0.11 eV for the PEN:F4-PEN I blends. Simulations confirm these numbers and are discussed below. We finally note that the slightly stronger scattering of the IE values for the PEN:F4-PEN II blends can be explained by the different growth behavior of this derivative. F4-PEN II exhibits a strong island growth, such that large areas of the substrate are not covered as shown by atomic force microscopy (AFM) measurements (see Supporting Information).

We wish to emphasize that the shift measured for the PEN:F4-PEN I blend is not only larger than the previously reported shifts in zinc phthalocyanine (ZnPc) mixtures,^[2]

but also, that the shift per fluorine atom is extremely high. A comparison of these values can be found in Figure 4. Blends with F4-PEN II, on the other hand, achieve overall the lowest absolute energy shift and energy shift per fluorine atom. This fact highlights that not only the number of fluorine atoms, but also their positions have a major impact on the effect of energy level tuning.

2.4. Simulations of the Energetic Properties of Blended Films

To obtain a deeper understanding of the origin of the strong shift of the IE for the PEN:F4-PEN I blend and the rather

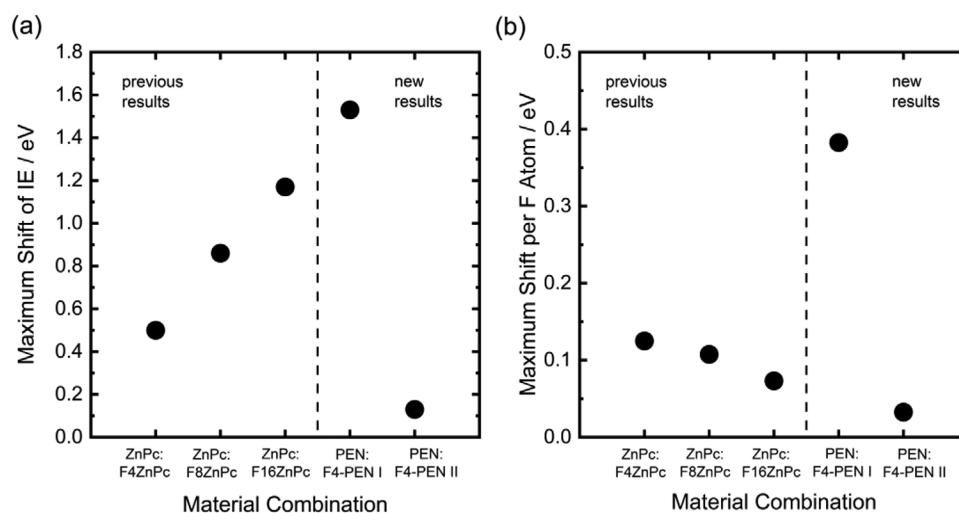


Figure 4. IE shifts of various blend systems. In comparison with previous published shifts in ZnPc blends,^[2] the blends containing F4-PEN I do not only reach a) the largest shift of the IE but also b) the highest shift per fluorine atom. In contrast, blends with F4-PEN II exhibit the lowest absolute shift and the lowest shift per fluorine atom.

weak shift for the PEN:F4-PEN II blend, we perform simulations of the electrostatic crystal fields for the respective systems. We therefore generated model slabs of varying size for molar pentacene ratios of $c = 0\%$, 25% , 50% , 75% , and 100% . For each mixing ratio, we calculate the electrostatic energy Φ_c of a single excess charge centered on the respective molecule (PEN, F4-PEN I, or F4-PEN II) and surrounded by other neutral molecules. The contribution of each molecule to Φ_c is modeled based on their atomic charges. This approach allows not only to include the quadrupole moments (Table 1) but also higher moments of the molecular charge distribution. Detailed information on the model can be found in the Experimental Section. The ionization energy IE_c in the respective blend is obtained as $IE_c = IE_0 + \Phi_c$, where IE_0 is independent of the mixing ratio and is chosen such that the IE_c matches the experimental values at a 50:50 ratio. Figure 3 shows the resulting ionization energy IE_c (open symbols) for the PEN:F4-PEN I blend (a) and the PEN:F4-PEN II blend (b). For both blend systems we find an excellent quantitative agreement for the shift in the IE, which is more than 1.2 eV for the PEN:F4-PEN I blend but only about 0.1 eV for the PEN:F4-PEN II blend. Because the simulated shift is exclusively due to the energy Φ_c , we can conclude that the shift of the experimental ionization energy is indeed caused by electrostatic potentials from the crystal field.

A more detailed understanding based on these potentials can be obtained from Figure 5 where the different molecular electrostatic potentials of PEN, F4-PEN I, and F4-PEN II are illustrated (Figure 5a–c). While PEN and F4-PEN II show positive isosurfaces in both x and y direction, F4-PEN I shows a completely different structure with a negative isosurface in y direction. In the crystal geometry with herringbone-fashion, this translates to specific interactions to the nearest neighbor molecules. In

Figure 5d–f, we select two neighboring molecules in the herringbone plane to show their impact on a given molecule in the center. The positive potential (red) in the molecular plane of F4-PEN I attracts the electrons on the neighboring molecules in the same herringbone plane, causing an increase of the ionization energy. This attraction is much weaker for PEN as neighboring molecules (see Figure 5d), explaining the decrease of the ionization energy with increasing content of PEN. In contrast, the IE change is marginal for the PEN:F4-PEN II blend due to similar potentials. This picture does not change significantly in the case of a different stacking in an F4-PEN II dominated PEN:F4-PEN II blend.

2.5. Investigations of the Charge Carrier Transport and Charge Injection Properties

In addition to the strong influence on the electronic properties, these electrostatic effects are expected to severely influence the charge carrier transport in devices based on such blended films. In order to investigate this influence in detail, we analyze the charge carrier transport in blended layers of PEN and F4-PEN I in organic field-effect transistors with a staggered bottom-gate configuration (see Supporting Information for details of the device structure). We have chosen selective electrodes (Al and Au) in order to study electron and hole transport separately. It was not possible to measure transistors with F4-PEN II since the strong island growth prevented the formation of closed layers.

We first analyze the charge carrier transport from the transfer characteristic of the blended films, allowing to derive the field-effect mobility (Table 3). The charge carrier mobility is determined for long channel devices ($L = 150 \mu\text{m}$) to reduce

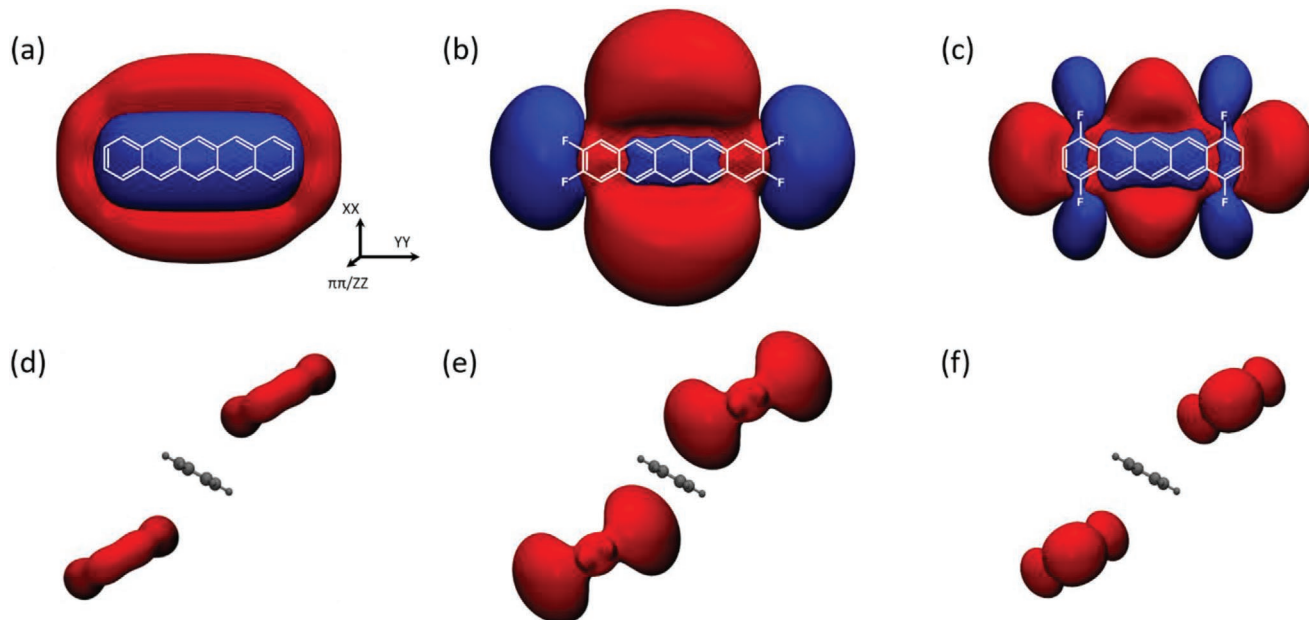


Figure 5. a–c) Electrostatic isopotential surfaces of gas phase molecules in herringbone arrangement. The blue (red) features represent negative (positive) regions. The isosurface value is ± 0.1 V. d–f) Dominating (attractive) part of the electrostatic potential of nearest neighbor molecules in the herringbone structure. Its influence on a selected molecule in the center is by far the largest for F4-PEN I (e). The distance between molecules is increased for better visibility.

Table 3. Mobility for different mixing ratios obtained from the linear regime of the output characteristics for different metal source/drain electrodes of aluminum or gold.

Electrode	Carrier type	PEN	3:1	1:1	1:3	F4-PEN I
Al	Electron	–	0.005	0.04	0.006	0.06
	Hole	–	0.03	–	–	–
Au	Electron	–	–	–	0.02	–
	Hole	0.5	0.04	0.01	–	–

Carrier mobility [$\text{cm}^2 \text{V}^{-1} \text{s}^{-1}$] in neat systems and blends

the influence of the contacts. The devices with pure PEN and F4-PEN I show an almost ideal behavior (see Figure S3, Supporting Information) allowing for an extraction of the charge carrier mobility of 0.5 and 0.06 $\text{cm}^2 \text{V}^{-1} \text{s}^{-1}$, respectively, within the limits of the gradual channel approximation. Upon blending PEN with the fluorinated derivatives, the transfer curves differ from the ideal transistor behavior originating either from a charge carrier dependent mobility (e.g., as a consequence of trap states) or an injection limitation at the contacts. In any case, the reduced slope of the transfer curves suggests a significant drop in mobility from 0.5 $\text{cm}^2 \text{V}^{-1} \text{s}^{-1}$ for the pure PEN film to 0.04 $\text{cm}^2 \text{V}^{-1} \text{s}^{-1}$ for 75% of PEN and 0.01 $\text{cm}^2 \text{V}^{-1} \text{s}^{-1}$ for 50% of PEN. A similar behavior is observed for the electron transport in F4-PEN I where the electron mobility drops from 0.06 $\text{cm}^2 \text{V}^{-1} \text{s}^{-1}$ for 100% F4-PEN I by more than one order of magnitude for the blended films. However, in both cases, such a strong drop of the hole/electron mobility is not expected for mixing ratios of 1:3/3:1 because in an ideally intermixed molecular system there should be still a sufficient number of possible percolation paths supporting the transport of charge carriers. It is therefore interesting to study where this strong drop of mobility comes from.

In order to answer this question, we focus on the output characteristics of these transistors (Figure 6). At first glance, the curves in both graphs look almost ideal. However, in an ideal, long-channel, metal–insulator–semiconductor thin-film

transistor, the saturation regime begins once $|V_{\text{DS}}| = |V_{\text{GS}} - V_{\text{th}}|$ is fulfilled. Here, V_{DS} is the drain-source voltage, V_{GS} the gate-source voltage, and V_{th} the threshold voltage. Hence, the point of saturation (pinch-off point) should therefore shift with changing gate-source bias. This condition holds true for the pure F4-PEN I or pure PEN device, which enables a correct extraction of charge mobility for pure films. However, the device containing a blended layer shows only little change of the apparent pinch-off point on the gate-source bias (see Figure 6b) and hence, the extraction of charge carrier mobility through the slope of the transfer curves is not possible. This non-ideality of the transistor behavior for blended films can have various reasons, such as a more complex field dependent or charge carrier density dependent carrier mobility in the blended films, which might be caused, for example, by a varying degree of disorder in the different blends. However, here it most likely stems from non-ohmic charge carrier injection (so-called source-gated transistors).^[20,21] Considering an equivalent circuit of the device consisting of a contact diode, contact resistor R_{co} and channel resistor R_{ch} (inset in Figure 6b), the characteristics of an ideal transistor are governed by the (controllable) channel resistance while the other components of the equivalent circuit are negligible. This results in the close to ideal characteristics observed for the pure materials. For the blended films though, where the pinch-off point does not shift with V_{GS} , the contact diode seems to dominate the output characteristics, indicating

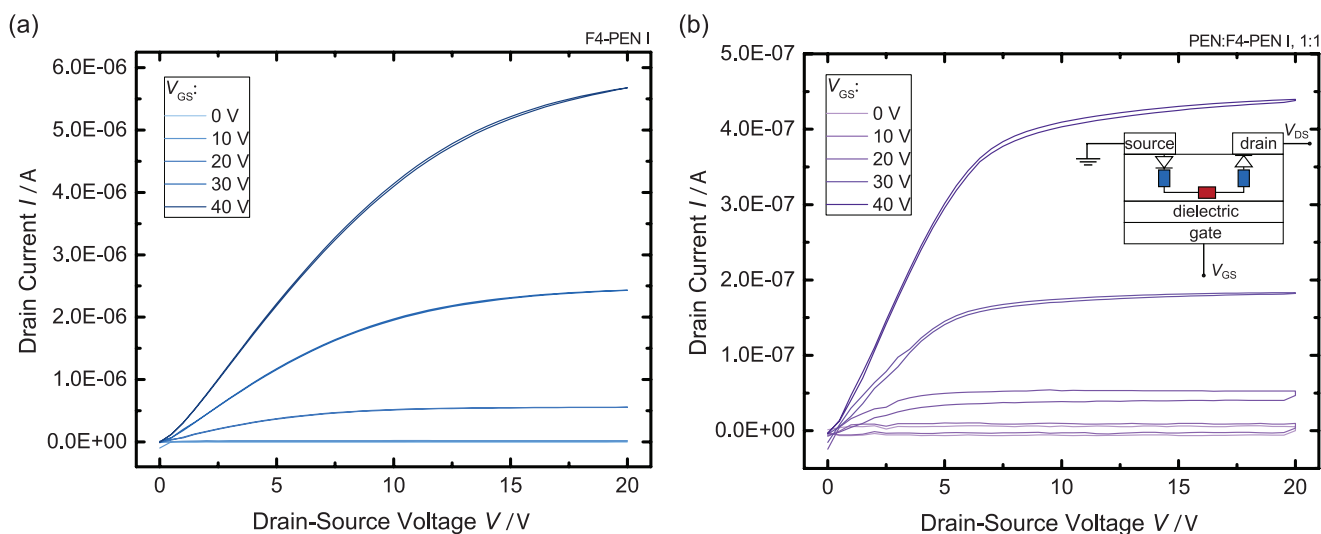


Figure 6. Output curves of OFETs with a) pristine F4-PEN I or b) a 1:1 blend of F4-PEN I and PEN as the semiconductor indicate a shift of the energy levels. The inset in (b) shows an equivalent circuit of a transistor with contact diodes, the contact resistances R_{co} behind the diodes (blue) and the resistance of the channel R_{ch} (red).

a mismatch of the work function of the source/drain metal and the IE of the semiconductor. This mismatch results in a large voltage drop across the contact diode and a low voltage drop across the channel—a typical behavior of source-gated transistors where an energy barrier is intentionally employed at the source-semiconductor interface.^[20,21] Such devices show a comparably constant pinch-off point as the devices based on blended films studied here. Hence, the blended devices exhibit an energy barrier that is created by shifting the transport levels, thus emphasizing the importance of energy level engineering for the transport in electronic devices. Most notably, the striking importance of this energy barrier is seen by the fact that despite their rather long channel of more than 50 μm (Figure 6), they show a very pronounced contact limitation. Although, we cannot exclude that disorder also influences the charge carrier injection, we believe that varying IE in the different blends due to energy-level engineering is the dominant mechanism. In principle, a more detailed analysis of the contact resistance (e.g., temperature dependence) should allow to extract the height of the Schottky-barrier at the contacts. However, due to the unknown temperature dependence of the charge carrier mobility (determining R_{ch}) and the contact diode, an unambiguous extraction of the Schottky barrier height in a two-probe transistor configuration is not possible. Nonetheless, our experiments clearly prove that energy level engineering by blending can be used to modify the charge carrier injection properties in organic field-effect transistors.

3. Conclusion

In this work, we demonstrate the strong effect of molecular charge distributions on energy level engineering in blends based on pentacene and two differently fluorinated derivatives. We verify by X-ray diffraction that the blends of PEN:F4-PEN I exhibit a suitable mixing behavior for energy level engineering due to the absence of phase separation. The ionization energy in the PEN:F4-PEN I blend can be tuned by more than 1.2 eV by varying the mixing ratio, which is the largest value reported up to now. This fact shows that the quadrupole effect can be scaled to a much larger energy scale than found before. Simulations support these findings and reveal that the shift of the IE is based on changes in the molecular electrostatic potentials due to changes of the charge distribution of the molecules upon halogenation. Small changes in the structure of the molecules such as the position of the fluorine atoms thus has an enormous influence on the tuning of electronic structures in organic semiconductors. Furthermore, measurements on OFET confirmed the findings of the energy level shift qualitatively.

4. Experimental Section

Grazing Incidence Wide-Angle X-Ray Scattering: The GIWAXS experiments were conducted at beamline SixS of the synchrotron radiation source SOLEIL in Gif-sur-Yvette, France. The X-ray energy was set to 12 keV, the angle of incidence α_i was 0.2° and sample to detector distance was set to 1177 mm. Hybrid pixel detector XPAD with 130 \times 130 μm pixel size was used to acquire the GIWAXS patterns. The integration time for the detector was set to 0.3 s per step. The

measurements were carried out in so called fly mode, where the detector on the diffractometer arm moved in series of in-plane 2θ scans (15 degrees in 1000 steps) for set range of out-of-plane angles (7 degrees in 7 steps). The investigated layers with thickness 20 nm were prepared on Si wafers with native SiO_x layer on the top.

Ultraviolet Photoelectron Spectroscopy: The UPS spectra were obtained by a PHOIBOS 100 analyzer system (Specs, Berlin, Germany) at a base pressure of 10^{-11} mbar using He I excitation lines (21.22 eV). The energy resolution of the setup was of around 150 meV but repeating the sample production under the same experimental conditions gave an experimental uncertainty of 70 meV. The spectra were calibrated to the Fermi edge of silver substrates. All samples were produced by thermal (co-)evaporation in UHV at a base pressure of 10^{-8} mbar using individual quartz crystal monitors for each material. Rates of 0.1–0.2 $\text{\AA} \text{ s}^{-1}$ and sputter-cleaned silver foils covered with 5 nm of p-doped BPAPF (5 wt%, doped with NDP9—a commercial p-dopant by Novalde GmbH, Germany) were used as substrates. The investigated layers had a thickness of 20 nm.

Atomic Force Microscopy: AFM images were obtained with an AIST-NT Combiscope1000 using TAP-AI-G tips from budget sensors. The sample was prepared by thermal (co-)evaporation in UHV using Si with native SiO_x covered with 5 nm BPAPF doped with NDP9 (5 wt%) as substrate. The nominal film thickness was 20 nm.

OFET: The samples for the electrical OFET measurements were prepared on a strongly doped Si substrate, which also served as a global gate electrode, covered with a 100 nm thick layer of SiO₂ and 40 nm of Cytop. The semiconductor materials were (co-)evaporated in a UHV chamber at a base pressure of 10^{-8} mbar. The metal contacts were structured by using a stainless steel shadow mask during evaporation, yielding channel dimensions of $W = 1000 \mu\text{m}$ (width) and $L = 50\text{--}150 \mu\text{m}$ (length). The measurements were performed in nitrogen atmosphere with a Keithley 2400 and a Keithley 2601 SMU for gate and drain bias, respectively. The inert atmosphere was not broken during handling.

Simulation - Determination of the Crystal Structures: The model co-crystals for different mixing ratios of PEN and its fluorinated derivatives (F4-PEN I or F4-PEN II) were primarily created on the basis of the experimental PEN crystal structure.^[19] The original unit cell consisting of two molecules was doubled to obtain a unit cell consisting of four molecules. Depending on the desired mixing ratio of the co-crystals, one (25%), two (50%), three (75%), or four (100%) PEN molecules were substituted by the respective fluorinated derivative. In contrast to PEN and F4-PEN I, pure F4-PEN II did not crystallize in a herringbone fashion, but a π -stack structure.^[17] Therefore, this structure was used to generate the pure F4-PEN II crystal and the 75% F4-PEN II blend, assuming that at higher concentrations of PEN the PEN herringbone structure prevailed.

Subsequently, the atomic coordinates and lattice vectors were optimized for a periodic crystal with density functional theory (DFT) at the PBE^[22,23] level of theory based on the projector augmented wave method^[24,25] as implemented in VASP.^[26–29] Dispersion corrections were known to be important for molecular structures^[30] and were included based on Grimme's DFT-D3 method.^[31] An increase of the volume of the unit cell (as compared to pristine PEN) with an increasing content of F4-PEN was observed similar to the experimental trend.

Simulation - Determination of the Energetic Correction Due to the Crystal Field: To calculate the energetic correction to the ionization potential Φ_{e} , finite slab systems of the size of 100 nm \times 100 nm \times 20 nm were constructed for each mixing ratio, where the z-axis of the slab corresponded to the long axis of the PEN molecules. The molecule that carried the excess-charge was placed at the surface in z-direction and in the center of the x-y plane.

For this center molecule, the surrounding slab was divided into an inner and outer region. The inner region consisted of the center molecule and all nearest-neighbor molecules (first shell). The contribution of the inner region to the energetic correction Φ_{in} was calculated with DFT and the contribution of the outer region Φ_{out} was obtained with a classical approach. To calculate the energetic response of the nearest-neighbor shell upon charging the center molecule, single-point constraint DFT

(cDFT) calculations were performed, where the charging state of the center molecule was constrained to either neutral or positively charged. For each charging state, the total DFT energy of the inner region (E_{in}^{neu} and E_{in}^{cat}) and the total DFT energy of the single center molecule (E_{center}^{neu} and E_{center}^{cat}) were calculated. With these energies, the energetic response of the nearest-neighbor shell upon charging of the center molecule was calculated as:

$$\Phi_{in} = (E_{in}^{neu} - E_{center}^{neu}) - (E_{in}^{cat} - E_{center}^{cat}) \quad (1)$$

Here, the DFT calculations were performed with NWchem^[32] at the B3LYP^[33–36] level of theory and the 6–31G^{*(37,38)} basis set. Grimme's DFT-D3^[31] dispersion correction and the LB94 asymptotic correction were included.^[39]

The outer region consisted of all remaining molecules in the slab (beyond the nearest-neighbors of the center molecule). To calculate the contribution of the outer region to the energetic correction, the charge distribution of each molecule was decomposed into a collection of atomic charges (point charges located at the atomic positions) by means of DFT calculations as described below. The set of atomic charges of the center molecule changed upon charging. Accordingly, the energetic contribution of the outer region was calculated as the screened monopole–monopole interaction energy of all atomic charges in the slab with the charge difference between the neutral and the charged configuration of the center molecule:

$$\Phi_{out} = \frac{1}{4\pi\epsilon_0} \sum_i^{center} \sum_j^{out} \frac{\Delta q_i \cdot q_j}{\epsilon |r_i - r_j|} + \Phi_{image} \quad (2)$$

$$\Phi_{image} = \frac{1}{4\pi\epsilon_0} \sum_i^{center} \sum_j^{out} \frac{\Delta q_i' \cdot q_j}{\epsilon |r_i' - r_j|} \quad (3)$$

where the sum i runs over all atoms of the center molecule and the sum j runs over all atoms of the molecules in the outer region. Here, each atom was characterized by a position vector r_i and an atomic charge q_i , which were taken from DFT calculations. Since the energy difference was calculated upon charging the center molecule, only the excess charge $\Delta q_i = q_i^{neu} - q_i^{cat}$ of its atoms entered into Equation (2). ϵ_0 is the vacuum permittivity and ϵ is the dielectric constant of the slab. Since the excess charge was located near the surface of the slab (interfaced to air), the image-charge correction Φ_{image} generated by the image charges $\Delta q_i' = \frac{\epsilon-1}{\epsilon+1} \Delta q_i$ located at r_i' above the surface with the same distance to the surface as the original charge Δq_i was included according to the classical electrostatics at dielectric–vacuum interfaces. The isotropic dielectric constant of the slab ϵ was calculated as the geometric mean of the dielectric tensor calculated with VASP^[40] for each analyzed mixing ratio. For the pure pentacene slab a dielectric constant of $\epsilon = 3.9$ was obtained, which fitted well to the range of experimental values.^[41]

It was found that the dielectric constant changed slightly with the mixing ratio of the slab. To account for the resulting change in the polarization response on the excess charge P_{out} the polarization response for each mixing ratio was calculated as:

$$P_{out} = \int dV |E_{vac}(r)|^2 - \epsilon \int dV |E_{med}(r)|^2 \quad (4)$$

with

$$E_{vac}(r) = \frac{1}{4\pi\epsilon_0} \sum_i^{center} \frac{\Delta q_i}{|r - r_i|^3} (r - r_i) q \quad (5)$$

and

$$E_{med}(r) = \frac{1}{4\pi\epsilon_0} \sum_i^{center} \frac{\Delta q_i}{\epsilon |r - r_i|^3} (r - r_i) + \frac{1}{4\pi\epsilon_0} \sum_i^{center} \frac{\Delta q_i'}{\epsilon |r - r_i'|^3} (r - r_i') \quad (6)$$

The integration was performed over the full slab excluding the volume of the inner shell by means of Monte-Carlo integration and 100 million integration steps. The volume of the inner shell was excluded, since the polarization response of the inner shell was already included in the DFT calculation.

The final energetic correction due to the crystal field was finally obtained as the sum of the three contributions of the inner and outer regions as:

$$\Phi_c = \Phi_{in} + \Phi_{out} + P_{out} \quad (7)$$

Simulation - Determination of Atomic Charges: The atomic charges used to calculate the screened monopole–monopole interaction in Φ_{out} (Equation (2)) were obtained by an electrostatic potential fit^[40,42] as implemented in Gaussian 16.^[43] The DFT calculations were performed in gas-phase at the B3LYP^[33–36] level of theory and with the 6–311++G^{*(37,38,44)} basis set.

Simulation - Calculation of the Ionization Energy and Quadrupole Moments: All properties were calculated with DFT in gas-phase using the Gaussian 16 package.^[43] The PEN, F4-PEN I, and F4-PEN II geometries were prerelaxed in their neutral state using B3LYP^[33–36] and the 6–311G^{**} basis set.^[37,38] The quadrupole moments and the energy of the neutral molecule E_{neu} , as well as the energy of the charged molecule E_{cat} , were calculated at the M06-2X^[45] level of theory and the cc-pVTZ basis set^[46] for the neutral relaxed geometry. The vertical ionization energy was finally calculated as

$$IE = |E_{neu} - E_{cat}| \quad (8)$$

Supporting Information

Supporting Information is available from the Wiley Online Library or from the author.

Acknowledgements

K.O. and K.L. acknowledge financial support by the German Research Foundation (DFG) (project LE 747/60-1) and the Graduate Academy of TU Dresden. S.H. would like to thank Studentenwerk Dresden for funding through the Saxony State Scholarship program. Additionally, the authors acknowledge the Alexander von Humboldt foundation for the financial support of M.H. The authors further acknowledge SOLEIL for provision of synchrotron radiation facilities and would like to thank Alessandro Coati for assistance in using beamline SixS. Moreover, F.O. would like to thank the DFG for funding through projects OR 349/1 and OR 349/3 and the Zentrum für Informationsdienste und Hochleistungsrechnen of TU Dresden (ZIH) for grants of computing time.

Conflict of Interest

The authors declare no conflict of interest.

Keywords

charge carrier transport, energy level tuning, long-range electrostatic forces, organic electronics, structure-property relationship

Received: April 3, 2020
Revised: April 28, 2020
Published online: June 22, 2020

- [1] S. M. Sze, K. K. Ng, *Physics of Semiconductor Devices*, Wiley, Hoboken, NJ **2007**.
- [2] M. Schwarze, W. Tress, B. Beyer, F. Gao, R. Scholz, C. Poelking, K. Ortstein, A. A. Guenther, D. Kasemann, D. Andrienko, K. Leo, *Science* **2016**, 352, 1446.
- [3] M. Schwarze, K. S. Schellhammer, K. Ortstein, J. Benduhn, C. Gaul, A. Hinderhofer, L. P. Toro, R. Scholz, J. Kublitski, S. Roland, M. Lau, C. Poelking, D. Andrienko, G. Cuniberti, F. Schreiber, D. Neher, K. Vandewal, F. Ortman, K. Leo, *Nat. Commun.* **2019**, 10, 2466.
- [4] A. Opitz, B. Ecker, J. Wagner, A. Hinderhofer, F. Schreiber, J. Manara, J. Pflaum, W. Brütting, *Org. Electron.* **2009**, 10, 1259.
- [5] A. Opitz, J. Wagner, W. Brütting, A. Hinderhofer, F. Schreiber, *Phys. Status Solidi A* **2009**, 206, 2683.
- [6] A. Hinderhofer, F. Schreiber, *ChemPhysChem* **2012**, 13, 628.
- [7] A. Hinderhofer, C. Frank, T. Hosokai, A. Resta, A. Gerlach, F. Schreiber, *J. Chem. Phys.* **2011**, 134, 104702.
- [8] V. Belova, P. Beyer, E. Meister, T. Linderl, M.-U. Halbich, M. Gerhard, S. Schmidt, T. Zechel, T. Meisel, A. V. Generalov, A. S. Anselmo, R. Scholz, O. Konovalov, A. Gerlach, M. Koch, A. Hinderhofer, A. Opitz, W. Brütting, F. Schreiber, *J. Am. Chem. Soc.* **2017**, 139, 8474.
- [9] A. Opitz, J. Wagner, W. Brütting, I. Salzmann, N. Koch, J. Manara, J. Pflaum, A. Hinderhofer, F. Schreiber, *IEEE J. Sel. Top. Quantum Electron.* **2010**, 16, 1707.
- [10] I. Salzmann, S. Duhm, G. Heimel, J. P. Rabe, N. Koch, M. Oehzelt, Y. Sakamoto, T. Suzuki, *Langmuir* **2008**, 24, 7294.
- [11] K. Broch, M. Gerhard, M. Halbich, S. Lippert, V. Belova, M. Koch, F. Schreiber, *Phys. Status Solidi* **2017**, 8, 1700064.
- [12] I. Salzmann, S. Duhm, G. Heimel, M. Oehzelt, R. Kniprath, R. L. Johnson, J. P. Rabe, N. Koch, *J. Am. Chem. Soc.* **2008**, 130, 12870.
- [13] R. Bula, I. M. Oettel, H. F. Bettinger, *J. Org. Chem.* **2012**, 77, 3538.
- [14] B. Shen, T. Geiger, R. Einholz, F. Reicherter, S. Schundelmeier, C. Maichle-Mössmer, B. Speiser, H. F. Bettinger, *J. Org. Chem.* **2018**, 83, 3149.
- [15] S.-A. Savu, G. Biddau, L. Pardini, R. Bula, H. F. Bettinger, C. Draxl, T. Chassé, M. B. Casu, *J. Phys. Chem. C* **2015**, 119, 12538.
- [16] S.-A. Savu, A. Sonström, R. Bula, H. F. Bettinger, T. Chassé, M. B. Casu, *ACS Appl. Mater. Interfaces* **2015**, 7, 19774.
- [17] T. Geiger, S. Schundelmeier, T. Hummel, M. Ströbele, W. Leis, M. Seitz, C. Zeiser, L. Moretti, M. Maiuri, G. Cerullo, K. Broch, J. Vahland, K. Leo, C. Maichle-Mössmer, B. Speiser, H. F. Bettinger, *Chem. - Eur. J.* **2020**, 26, 3420.
- [18] K. R. Graham, G. O. N. Ndjawa, S. M. Conron, R. Munir, K. Vandewal, J. J. Chen, S. Sweetnam, M. E. Thompson, A. Salleo, M. D. McGehee, A. Amassian, *Adv. Energy Mater.* **2016**, 6, 1601211.
- [19] S. Schiefer, M. Huth, A. Dobrinevski, B. Nickel, *J. Am. Chem. Soc.* **2007**, 129, 10316.
- [20] J. Zhang, J. Wilson, G. Auton, Y. Wang, M. Xu, Q. Xin, A. Song, *Proc. Natl. Acad. Sci. USA* **2019**, 116, 4843.
- [21] R. A. Sporea, M. J. Trainor, N. D. Young, J. M. Shannon, S. R. P. Silva, *Sci. Rep.* **2015**, 4, 4295.
- [22] J. P. Perdew, K. Burke, M. Ernzerhof, *Phys. Rev. Lett.* **1996**, 77, 3865.
- [23] J. P. Perdew, K. Burke, M. Ernzerhof, *Phys. Rev. Lett.* **1997**, 78, 1396.
- [24] P. E. Blochl, *Phys. Rev. B* **1994**, 50, 17953.
- [25] G. Kresse, D. Joubert, *Phys. Rev. B* **1999**, 59, 1758.
- [26] G. Kresse, J. Hafner, *Phys. Rev. B* **1993**, 47, 558.
- [27] G. Kresse, J. Hafner, *Phys. Rev. B* **1994**, 49, 14251.
- [28] G. Kresse, J. Furthmüller, *Comput. Mater. Sci.* **1996**, 6, 15.
- [29] G. Kresse, J. Furthmüller, *Phys. Rev. B* **1996**, 54, 11169.
- [30] F. Ortman, F. Bechstedt, W. G. Schmidt, *Phys. Rev. B* **2006**, 73, 205101.
- [31] S. Grimme, J. Antony, S. Ehrlich, H. Krieg, *J. Chem. Phys.* **2010**, 132, 154104.
- [32] M. Valiev, E. J. Bylaska, N. Govind, K. Kowalski, T. P. Straatsma, H. J. J. van Dam, D. Wang, J. Nieplocha, E. Apra, T. L. Windus, W. A. de Jong, *Comput. Phys. Commun.* **2010**, 181, 1477.
- [33] A. D. Becke, *J. Chem. Phys.* **1993**, 98, 5648.
- [34] C. Lee, W. Yang, R. G. Parr, *Phys. Rev. B* **1988**, 37, 785.
- [35] S. H. Vosko, L. Wilk, M. Nusair, *Can. J. Phys.* **1980**, 58, 1200.
- [36] P. J. Stephens, F. J. Devlin, C. F. Chabalowski, M. J. Frisch, *J. Phys. Chem.* **1994**, 98, 11623.
- [37] R. Ditchfield, W. J. Hehre, J. A. Pople, *J. Chem. Phys.* **1971**, 54, 724.
- [38] G. A. Petersson, A. Bennett, T. G. Tensfeldt, M. A. Al-Laham, W. A. Shirley, J. Mantzaris, *J. Chem. Phys.* **1988**, 89, 2193.
- [39] R. van Leeuwen, E. J. Baerends, *Phys. Rev. A* **1994**, 49, 2421.
- [40] C. H. Kim, O. Yaghmazadeh, D. Tondelier, Y. B. Jeong, Y. Bonnassieux, G. Horowitz, *J. Appl. Phys.* **2011**, 109, 083710.
- [41] U. C. Singh, P. A. Kollman, *J. Comput. Chem.* **1984**, 5, 129.
- [42] B. H. Besler, K. M. Merz Jr., P. A. Kollman, *J. Comput. Chem.* **1990**, 11, 431.
- [43] M. J. Frisch, G. W. Trucks, H. B. Schlegel, G. E. Scuseria, M. A. Robb, J. R. Cheeseman, G. Scalmani, V. Barone, G. A. Petersson, H. Nakatsuji, X. Li, M. Caricato, A. V. Marenich, J. Bloino, B. G. Janesko, R. Gomperts, B. Mennucci, H. P. Hratchian, J. V. Ortiz, A. F. Izmaylov, J. L. Sonnenberg, D. Williams-Young, F. Ding, F. Lipparini, F. Egidi, J. Goings, B. Peng, A. Petrone, T. Henderson, D. Ranasinghe, et al, Gaussian 16, Revision C.01, Gaussian, Inc., Wallingford CT **2016**.
- [44] T. Clark, J. Chandrasekhar, G. W. Spitznagel, P. v. R. Schleyer, *J. Comput. Chem.* **1983**, 4, 294.
- [45] Y. Zhao, D. G. Truhlar, *Theor. Chem. Acc.* **2008**, 120, 215.
- [46] T. H. Dunning Jr., *J. Chem. Phys.* **1989**, 90, 1007.